

pubs.acs.org/JPCL Letter

Benchmarking Quasiclassical Mapping Hamiltonian Methods for Simulating Cavity-Modified Molecular Dynamics

Maximilian A. C. Saller, Aaron Kelly, and Eitan Geva*



Cite This: J. Phys. Chem. Lett. 2021, 12, 3163–3170

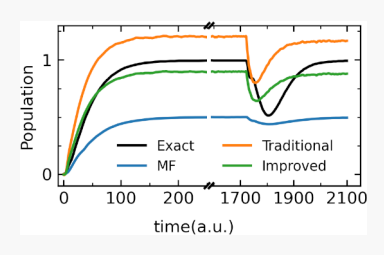


ACCESS I

Metrics & More

Article Recommendations

ABSTRACT: Recent experimental realizations of strong coupling between optical cavity modes and molecular matter placed inside the cavity have opened exciting new routes for controlling chemical processes. Simulating the cavity-modified dynamics of complex chemical systems calls for the development of accurate, flexible, and cost-effective approximate numerical methods that scale favorably with system size and complexity. In this Letter, we test the ability of quasiclassical mapping Hamiltonian methods to serve this purpose. We simulated the spontaneous emission dynamics of an atom confined to a microcavity via five different variations of the linearized semiclassical (LSC) method. Our main finding is that recently proposed LSC-



based methods which use a modified form of the identity operator are reasonably accurate and perform significantly better than the Ehrenfest and standard LSC methods, without significantly increasing computational costs. These methods are therefore highly promising as a general purpose tool for simulating cavity-modified dynamics of complex chemical systems.

INTRODUCTION

The recent experimental realization of strong 1-6 and ultrastrong⁷⁻¹⁰ coupling between optical cavity modes¹¹⁻¹⁴ and the electronic and vibrational degrees of freedom (DOF) of molecular matter has given rise to considerable interest in using this coupling to control and manipulate a wide variety of chemical and physical phenomena, including energy transfer, charge transfer, optical and electrical properties, nonlinear optical response, reactivity, photochemistry, and catalysis. 5,7,15-48 These experimental breakthroughs highlight the need for complementary computational approaches which can accurately and efficiently simulate the cavity-modified chemical dynamics. In contrast to the relatively simple model systems commonly used in quantum optics, ^{14,49–53} for which analytical solutions are often available, studying experimentally relevant systems in chemistry and biology requires approximate dynamics approaches which are accurate, computationally efficient, and not subject to the prohibitive exponential scaling of computational cost with system size limiting the use of quantum-mechanically exact numerical methods. The quasiclassical mapping Hamiltonian (QC/MH) approach⁵⁴ particularly promising in this respect, given its relative simplicity and the fact that it is rigorously derivable. 77,78 Multiple variations of the QC/MH approach have been proposed and applied over the years. 55,60-67,77-81 Notable examples include the mean-field Ehrenfest method^{55,81} and methods based on the linearized semiclassical (LSC) approximation.⁷⁷⁻⁸⁰ Considerable progress has recently been made in improving traditional QC/MH approaches, leading to the development of the symmetrical quasi-classical method⁶⁰⁻⁶⁵ and modified LSC (mLSC) methods, which are based on employing improved electronic population operators. 66,67

A systematic comparison of the accuracy of different QC/MH methods has been reported in several previous benchmark studies in the context of cavity-free molecular dynamics. ^{68,82} In this Letter, we report on what we believe is a first of its kind systematic comparison of the accuracy of QC/MH methods in the context of cavity-enabled molecular dynamics. To this end, we use a benchmark model consisting of a single stationary atom in a 1D lossless cavity undergoing spontaneous emission. ^{41,42}

■ MAPPING HAMILTONIAN METHODS

A detailed discussion of the various QC/MH methods we will benchmark here can be found in our previous work.⁶⁸ Below, we restrict ourselves to a brief overview of the relevant main results.

The overall system Hamiltonian is assumed to have the following generic form (in what follows, boldfaced variables, for example \mathbf{A} , indicate vector quantities, and a hat over a variable, for example $\hat{\mathbf{B}}$, indicates an operator quantity):

$$\hat{H} = \frac{\hat{\mathbf{p}}^2}{2} + \sum_{\alpha',\alpha=1}^{N_c} V_{\alpha'\alpha}(\hat{\mathbf{R}}) |\alpha'\rangle\langle\alpha|$$
(1)

Received: January 15, 2021 Accepted: March 16, 2021



Here, $\hat{\mathbf{R}}$ and $\hat{\mathbf{P}}$ are vector operators that represent the entire set of N_n mass-weighted nuclear coordinates and momenta, with the N_p canonical coordinates and momenta associated with the cavity modes (the so-called photonic DOF). The electronic Hilbert space is N_e -dimensional and spanned by the diabatic basis $\{|\alpha\rangle\}$. $V_{\alpha\alpha}(\mathbf{R})$ is the potential energy surface (PES) that corresponds to the α -th diabatic electronic state and $V_{\alpha\alpha'}(\hat{\mathbf{R}})$ is the coupling between the α -th and α' -th electronic states ($\alpha \neq$ α'). It should be noted that both $\{V_{\alpha\alpha}(\hat{\mathbf{R}})\}$ and $\{V_{\alpha\alpha'}(\hat{\mathbf{R}})\}$ can depend on the coordinates associated with both nuclear and photonic DOF, which play similar roles. Thus, conceptually, the inclusion of the cavity modes corresponds to having additional nuclear-like DOF. 32,83 It should also be noted that the choice of a diabatic electronic basis is a matter of convenience (the QC/MH methods discussed in this Letter can be formulated in terms of other electronic bases, including the adiabatic basis⁸⁴).

Since our focus in this paper is on simulating the dynamics of spontaneous emission, it is natural to focus on the dynamics of the populations of the above-mentioned diabatic electronic states. We will also restrict ourselves to the cases where the initial state of the overall system is separable and given by $\hat{\rho}_{np}\lambda\rangle\langle\lambda l$, where $\hat{\rho}_{np}$ and $\lambda\rangle\langle\lambda l$ are the density operators that represent the initial states of the nuclear+photonic and electronic DOF, respectively (where λ) is one of the diabatic states). Under these uncorrelated conditions, the population of the diabatic state λ at a later time λ is given by the following correlation function:

$$C_{\lambda\alpha}(t) = \text{Tr}[\hat{\rho}_{np}|\lambda\rangle\langle\lambda|e^{i\hat{H}t}|\alpha\rangle\langle\alpha|e^{-i\hat{H}t}]$$
(2)

As outlined in refs 66 and 67, the electronic population operator can be mapped as the sum of the electronic identity operator, $\hat{1}$, and a trace zero operator, \hat{Q}_{α} such that

$$\begin{split} |\alpha\rangle\langle\alpha| &= \frac{1}{N_e}[\hat{1} + \hat{Q}_{\alpha}] \qquad \text{where} \\ \hat{Q}_{\alpha} &= N_e |\alpha\rangle\langle\alpha| - \sum_{\alpha'=1}^{N_e} |\alpha'\rangle\langle\alpha'| \end{split} \tag{3}$$

Thus, one has the choice of working with either $|\alpha\rangle\langle\alpha|$ or \hat{Q}_{α} as the population operator. Substituting this alternative form of the population operator into the correlation function in eq 2 yields the following expression for the population of the diabatic state $|\alpha\rangle$ at a later time t in terms of the correlation functions $C_{\hat{1}\hat{Q}_{\alpha}}(t)$ and $C_{\hat{Q},\hat{Q}_{\alpha}}(t)$:

$$C_{\lambda\alpha}(t) = \frac{1}{N_e^2} (N_e + C_{\hat{1}\hat{Q}_{\alpha}}(t) + C_{\hat{Q}_{\lambda}\hat{Q}_{\alpha}}(t))$$
 (4)

In order to arrive at the QC/MH methods employed here, the electronic population operators are mapped onto a set of isomorphic operators, which are given in terms of so-called mapping variables. While the choice of mapping variables is not unique, in the popular Meyer–Miller–Stock–Thoss approach, employed in the derivation of the QC/MH methods studied in this Letter, the set of N_e electronic states is mapped onto an isomorphic set of N_e independent harmonic oscillators. The electronic population operators can then be cast in terms of the corresponding N_e harmonic oscillator Cartesian coordinates, $\hat{\bf q}=(\hat{q}_1,...,\hat{q}_N)$, and momenta.

$$\hat{\mathbf{p}} = (\hat{p}_1, ..., \hat{p}_{N_e})$$
, such that

$$|\alpha\rangle\langle\alpha| \to \frac{1}{2\hbar}(\hat{q}_{\alpha}^2 + \hat{p}_{\alpha}^2 - \hbar)$$
 (5)

The mapping relation in eq 5 is denoted mapping #1.

Alternatively, it is possible to instead map the electronic population operators onto the subspace of singly excited oscillator (SEO) states, such that

$$|\alpha\rangle\langle\alpha|\rightarrow|0_1,\,...,\,1_\alpha,\,...,\,0_{N_c}\rangle\langle0_{N_c},\,...,\,1_\alpha,\,...,\,0_1| \tag{6}$$

where each harmonic oscillator is in its ground state, with the exception of the α -th oscillator, which is in its first excited state. The mapping relation in eq 6 is denoted *mapping* #2.

Within the LSC approximation, $^{77-80}$ the aforementioned correlation function, $C_{\lambda\alpha}(t)$, is approximated by the following classical-like correlation function:

$$C_{\lambda\alpha}(t) pprox rac{1}{(2\pi)^{N_n+N_p+N_e}} \int \mathrm{d}\mathbf{q}_0 \int \mathrm{d}\mathbf{p}_0 \int \mathrm{d}\mathbf{R}_0 \int \mathrm{d}\mathbf{P}_0$$

$$[\hat{\rho}_{np}]_{W}(\mathbf{R}_{0}, \mathbf{P}_{0})[\lambda]\langle\lambda|]_{W}(\mathbf{q}_{0}, \mathbf{p}_{0})[\lambda]\langle\alpha|]_{W}(\mathbf{q}_{t}, \mathbf{p}_{t})$$
(7)

Similar expressions can be obtained for the correlation functions $C_{\hat{1}\hat{Q}_a}(t)$ and $C_{\hat{Q}_a\hat{Q}_a}(t)$. Here, $[\hat{\rho}_{np}]_W(\mathbf{R},\mathbf{P})$, $[l\lambda\rangle\langle\lambda l]_W(\mathbf{q},\mathbf{p})$ and $[l\alpha\rangle\langle\alpha l]_W(\mathbf{q},\mathbf{p})$ are the Wigner transforms of the corresponding operators, and $N_n+N_p+N_e$ is the overall number of DOF (nuclear + photonic + electronic). Importantly, $\{\mathbf{R}_t\mathbf{P}_t\mathbf{q}_t\mathbf{p}_t\}$ are obtained, starting at the initial state $\{\mathbf{R}_0,\mathbf{P}_0,\mathbf{q}_0,\mathbf{p}_0\}$, via classical dynamics based on the classical limit of the overall system Hamiltonian in eq 1 (in what follows, we will use the symmetrized mapping Hamiltonian for this purpose $^{55,66-68,86}$). It should be noted that evaluating the LSC approximation in eq 7 requires sampling over the initial conditions, $\{\mathbf{R}_0,\mathbf{P}_0,\mathbf{q}_0,\mathbf{p}_0\}$, and averaging over multiple classical trajectories.

While mappings #1 and #2 are freely interchangeable when a quantum-mechanically exact treatment is employed, this is not the case when the LSC approximation is applied. More specifically, the Wigner transforms of the electronic population operator are given by the following distinctly different classical-like expressions depending of whether *mapping #1* or *mapping #2* are used:

mapping #1:
$$[|\alpha\rangle\langle\alpha|]_W^{(1)}(\mathbf{q}, \mathbf{p}) = \frac{1}{2\hbar}(q_\alpha^2 + p_\alpha^2 - \hbar)$$
 (8)

mapping #2:
$$[|\alpha\rangle\langle\alpha|]_W^{(II)}(\mathbf{q}, \mathbf{p}) = \phi(\mathbf{q}, \mathbf{p}) \left(q_\alpha^2 + p_\alpha^2 - \frac{\hbar}{2}\right)$$
(9)

where

$$\phi(\mathbf{q}, \mathbf{p}) = \frac{2^{N_{\epsilon}+1}}{\hbar} \exp\left[-\frac{1}{\hbar} \sum_{\alpha'=1}^{N_{\epsilon}} \left(q_{\alpha'}^2 + p_{\alpha'}^2\right)\right]$$
(10)

The two traditional LSC approaches are based on applying the LSC approximation to the correlation function $C_{\lambda\alpha}(t)$ (see eq 2). Both methods use mapping #2 for the $|\lambda\rangle\langle\lambda|$ time-zero operator. Two reasons for this are that one must project onto the physical (SEO) subspace at least once and that the $\phi(\mathbf{q},\mathbf{p})$ function provides a convenient, bounded phase-space distribution from which to sample the initial values of the mapping variables. The two traditional LSC approaches differ in their treatment of the time-t operator, $|\alpha\rangle\langle\alpha|$. The first method, which we denote LSC I (sometimes also referred to as PBME⁸⁷), uses mapping #1 at time-t, whereas the second,

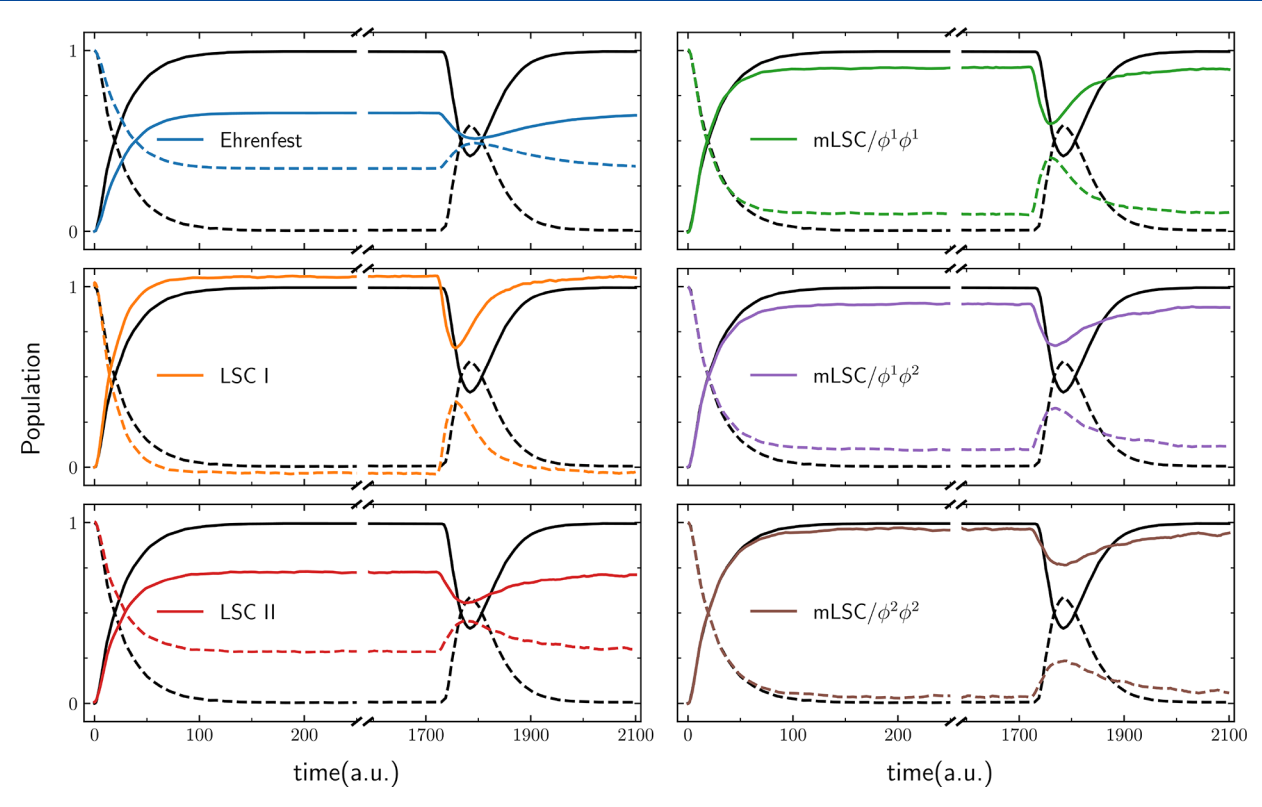


Figure 1. Atomic populations of the two-level system from QC/MH methods, compared to quantum mechanically exact benchmark data, 41,42 shown in black. Ground- and excited-state populations are shown as solid and dashed lines, respectively.

denoted LSC II (also known as LSC-IVR 57,58), uses *mapping* #2 at time-*t* as well as time-zero.

The mLSC methods, first introduced in refs 66 and 67 and expanded upon in ref 68, are based on applying the LSC approximation to the correlation functions $C_{\hat{1}\hat{Q}_a}(t)$ and $C_{\hat{Q}_a\hat{Q}_a}(t)$ (see eq 4). The first variation, referred to as mLSC/ $\phi^1\phi^1$, maps the identity operator to unity, $\hat{1}\rightarrow 1$, and employs mapping #1 for \hat{Q}_{λ} and mapping #2 for \hat{Q}_a . The second variation, referred as mLSC/ $\phi^1\phi^2$, also maps the identity to unity, but employs mapping #2 for both \hat{Q}_{λ} and \hat{Q}_a . The third variation, referred to as mLSC/ $\phi^2\phi^2$, maps the identity according to $\hat{1}\rightarrow 2\hbar\phi(\mathbf{q},\mathbf{p})$ and employs mapping #2 for both \hat{Q}_{λ} and \hat{Q}_a .

Finally, we note that the mean-field Ehrenfest method^{55,81} can also be formulated as a QC/MH method.⁵⁵ More specifically, Ehrenfest dynamics can be obtained from the same QC equations of motion that LSC-based methods give rise to. Where the Ehrenfest method differs from LSC approaches is in the way the mapping variables are sampled at the initial time and how electronic populations are calculated at a later time.

■ RESULTS AND DISCUSSION

In order to compare and contrast the performance of the six QC/MH methods outlined above (LSC I, LSC II, mLSC/ $\phi^1\phi^1$, mLSC/ $\phi^1\phi^2$, mLSC/ $\phi^2\phi^2$, and Ehrenfest), we applied them to two benchmark systems consisting of a stationary two-level or three-level atom placed in the center of a 1D lossless cavity of length L. It should be noted that the same models were previously used by Hoffmann et al. to benchmark other QC/MH methods. 41,42

The Hamiltonian for the atom-in-cavity model system under consideration is given by

$$\hat{H} = \sum_{\alpha=1}^{N_e} \varepsilon_{\alpha} |\alpha\rangle \langle \alpha| + \sum_{\alpha,\alpha'}^{N_e} \sum_{j=1}^{N_p} \mu_{\alpha\alpha'} \omega_j \lambda_j (R_S) \hat{R}_j |\alpha\rangle \langle \alpha'|$$

$$+ \frac{1}{2} \sum_{j=1}^{N_p} (\hat{P}_j^2 + \omega_j^2 \hat{R}_j^2)$$
(11)

where $\{\varepsilon_{\alpha}\}$ and $\{|\alpha\rangle\}$ are the energy levels and stationary states of the free atom; N_{e} and N_{p} are the numbers of atomic states and field modes respectively; $\mu_{\alpha\alpha'}$ is the transition dipole moment between atomic states $|\alpha\rangle$ and $|\alpha'\rangle$; ω_{j} is the frequency of the j-th cavity field mode (see eq 12 below), the canonical variables of which are given by \hat{R}_{j} and \hat{P}_{j} ; $\lambda_{j}(R_{S})$ is the coupling between the atom at position R_{S} and the j-th field mode (see eq 13 below). It should be noted that this model lacks explicit nuclear DOF and only includes electronic and photonic DOF.

The frequency of the j-th field mode is given by

$$\omega_j = \frac{jc\pi}{L}$$
 $j = 1,2,3, ..., N_p$ (12)

where c is the speed of light and L is the volume length of the cavity. The electron-photon coupling of the atom to the j-th field mode is given by

$$\lambda_{j}(R_{\rm S}) = \sqrt{\frac{2}{\varepsilon_0 L}} \sin(k_{j} R_{\rm S}) \tag{13}$$

where ε_0 is the vacuum permittivity and the wave vector of *j*-th field mode is given by $k_j = \omega_j/c = j\pi/L$. Following refs 41 and 42, we restrict ourselves to the special case where the atom is

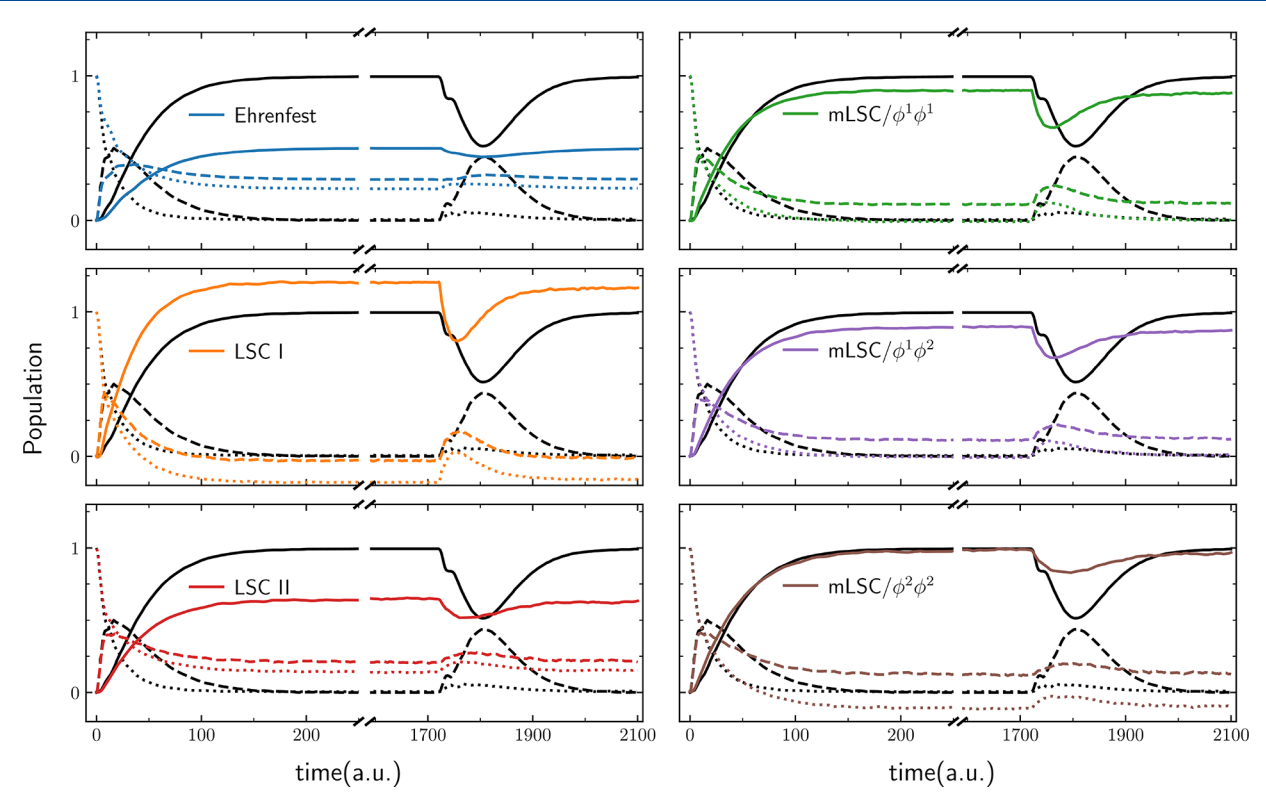


Figure 2. Atomic populations of the three-level system from QC/MH methods, compared to quantum mechanically exact benchmark data, 41,42 shown in black. Ground-, first and second excited-state populations are shown as solid, dashed and dotted lines, respectively.

placed at the center of the cavity $(R_S = L/2)$. As a result, the atom is decoupled from field modes with an even index, j = 2, 4, 6,

We employed the same parameter sets and initial conditions as in previous studies based on these benchmark systems. 32,41,42,88,89 In atomic units, these are $\varepsilon_1 = -0.6738$, ε_2 = -0.2798 and μ_{12} = 1.034 for the two-level system and ε_1 = -0.6738, $\varepsilon_2 = -0.2798$, $\varepsilon_3 = -0.1547$, $\mu_{12} = 1.034$ and $\mu_{23} =$ -2.536 for the three-level system. Note that in the latter system, the dipole moment operator only couples adjacent atomic states. In both systems, the atom is placed at the center $(R_S = L/2)$ of a 12.5 μ m cavity $(L = 2.362 \times 10^5 \text{ au})$, with 400 cavity modes taken into account. Note that, as mentioned above, due to the position of the atom at the center of the cavity, half of the aforementioned modes decouple, therefore reducing the number of modes for which dynamics are explicitly simulated to N_p = 200. The atomic system is initialized in its highest excited state, while initial conditions for the field modes are sampled from the Wigner transform of the field vacuum state

$$\left[\hat{\rho}_{np}\right]_{W}(\mathbf{R}, \mathbf{P}) = \prod_{j=1}^{N_{p}} \exp\left[-\frac{P_{j}^{2}}{\omega_{j}} - \omega_{j}R_{j}^{2}\right]$$
(14)

Finally, all results were obtained from simulations sampling over 10^5 QC trajectories, each of which 2.1×10^5 time steps long, with a duration of one time step given by 0.1 au, so that the total simulation time is 2100 a.u. (50.4 fs).

Figure 1 shows atomic populations of the two-level benchmark system obtained using mean-field Ehrenfest and traditional (LSC I and LSC II) as well as improved (mLSC/ $\phi^1\phi^1$, mLSC/ $\phi^1\phi^2$ and mLSC/ $\phi^2\phi^2$) QC/MH methods, compared with quantum mechanically exact configuration

interaction results (the latter were adopted from refs 41 and 42). On the qualitative level, all approximate methods seem to capture the main features of the population dynamics. More specifically, the system starts out with the atom in the excited state and the cavity field in the vacuum state. The initial decrease of the excited state population and increase of the ground state population corresponds to spontaneous emission. The emitted photon (or two photons in the case of the three-level system) travels toward the mirrors, where it is reflected, and then travels back to the atom. The emitted photon is then reabsorbed and re-emitted by the atom, which results in a positive (negative) spike in the excited (ground) state population.

On the quantitative level, the Ehrenfest mean-field approach clearly fails to capture the population dynamics of the two-level system, with considerable errors even at short times. It should be noted that this has already been shown to be the case by Hoffmann et al. 41,42 It should also be noted that Hoffmann et al. also found that the fewest switches surface hopping (FSSH) method, 90 which is often employed to overcome the shortcomings of the Ehrenfest method, performed even worse for this system. These failures provide a strong motivation for exploring alternative QC/MH methods, which we do next.

One such alternative QC/MH method is LSC I. However, as can be seen from Figure 1, LSC I still gives rise to short time errors and even more importantly yields unphysical populations greater than one and less than zero at longer times. Another alternative QC/MH method is LSC II. However, this method only produces marginal improvement over the Ehrenfest method and is still unable to accurately reproduce the exact results.

In contrast, the mLSC methods 66,67 constitute a consistent and significant improvement, not only over the mean-field result but also over the traditional LSC methods. mLSC/ $\phi^1\phi^1$ is comparable in accuracy to LSC I; however, importantly, it does not yield unphysical population values. mLSC/ $\phi^2\phi^2$ is more accurate than mLSC/ $\phi^1\phi^1$ with the exception of the population resurgence at $t\approx 1800$ a.u. mLSC/ $\phi^1\phi^2$ falls approximately in-between these two mLSC approaches. We note that mLSC/ $\phi^1\phi^1$ and mLSC/ $\phi^2\phi^2$ have also been found to yield the most accurate results for other benchmarks. $^{66-68,91}$

Figure 2 shows atomic populations for the three-level benchmark system, again obtained using mean-field Ehrenfest, LSC I and LSC II as well as the mLSC methods, compared to exact benchmark results. As in the two-level system, the mean-field Ehrenfest method fails to capture the population dynamics quantitatively, with considerable errors being present even at short times. The limitations of the LSC I approach become more apparent in the three-level system, where it yields considerable errors for both the ground and second excited state populations. Notably, these populations enter drastically unphysical regions, considerably above one and below zero, respectively. As in the two-level system, LSC II is only a marginal improvement over the mean-field result for the three-level system.

The mLSC methods again constitute a considerable improvement over mean-field and LSC II, but now, they also noticeably outperform LSC I. Out of the three mLSC methods, we consider mLSC/ $\phi^1\phi^1$ to be the most accurate, capturing all relevant aspects of the population dynamics without entering unphysical regions and maintaining a relatively high degree of accuracy with respect to the exact benchmark across the entire simulation time. Although mLSC/ $\phi^2\phi^2$ performs exceptionally well for the asymptotic limits of the ground state, we note the error in the populations of the first and second excited states, the latter of which spuriously falls below zero. mLSC/ $\phi^1\phi^2$ again appears to fall between the two other mLSC methods, though not exhibiting the aforementioned negative populations seen in mLSC/ $\phi^2\phi^2$.

Considering both benchmark systems, it is therefore clear that the mLSC QC/MH methods constitute a considerable improvement over traditional mean-field and LSC approaches. Overall, mLSC/ $\phi^1\phi^1$ appears to yield the best results for the atom-in-cavity benchmark systems studied here, in each case not only capturing the population dynamics with relative accuracy but also consistently outperforming traditional approaches. As in previous work, 66–58 we note that while mLSC/ $\phi^2\phi^2$ does outperform mLSC/ $\phi^1\phi^1$ in certain aspects and for certain systems, the latter is considered to generally be more reliable. Additionally, it is worth noting that the derivation of mLSC/ $\phi^2\phi^2$ is somewhat *ad hoc*.

CONCLUSIONS

Optical microcavities have recently been shown to have the potential to change the chemistry of systems placed within them. 1-6 Simulating the cavity-modified dynamics of complex chemical systems remains a formidable challenge. Exact quantum mechanical methods cannot be applied to realistic, experimentally relevant systems because of their unfavorable exponential scaling. 92-94 Approximate approaches with favorable scaling, such as the QC/MH class of methods under consideration here 54-76 remain largely unexplored in the context of matter-in-cavity systems. In this Letter, we report on what we believe is the first ever benchmark study of the ability

of six different QC/MH methods to capture cavity-modified dynamics.

We compared the performance of the traditional mean-field Ehrenfest approach, 55,81 two variations of the LSC method, LSC I and LSC II, 77-80 and a set of three mLSC methods employing improved population operators. 66-68 We find that the mLSC methods constitute a consistent and considerable improvement over the traditional Ehrenfest and LSC results. We also find that both Ehrenfest and LSC II are not able to accurately capture the population dynamics for either benchmark system, with the latter only constituting a small improvement over the former. While LSC I appears to be of similar accuracy to mLSC in the two-level system, although exhibiting small, unphysical errors in the populations, in the three-level system the difference between these approaches becomes more pronounced, with LSC I decreasing in accuracy, while mLSC retains its relative accuracy. Across both systems, we find mLSC/ $\phi^1\phi^1$ to be the most reliable approach, as has also been highlighted in previous work. 67,66

It should be noted that the fact that mLSC methods have been found to be significantly more accurate than both Ehrenfest and FSSH methods for the benchmark systems under consideration here is particularly encouraging. This is because the benchmark systems studied are gas-phase-like and the accuracy of mLSC methods is expected to improve in more condensed-phase-like chemical systems of increased system complexity.

The considerable increase in accuracy that can be achieved at no extra cost by using the mLSC methods over traditional LSC shows considerable promise for the study of matter-incavity systems going forward, especially for larger, more experimentally realistic systems. Extending the range of applicability of such QC/MH methods to photonic or polaritonic observables is also of considerable interest. Work on such extensions is underway and will be reported in future publications.

AUTHOR INFORMATION

Corresponding Author

Eitan Geva — Department of Chemistry, University of Michigan, Ann Arbor, Michigan 48109, United States; orcid.org/0000-0002-7935-4586; Email: eitan@umich.edu

Authors

Maximilian A. C. Saller – Department of Chemistry, University of Michigan, Ann Arbor, Michigan 48109, United States

Aaron Kelly – Max Planck Institute for the Structure and Dynamics of Matter, 22761 Hamburg, Germany; Department of Chemistry, Dalhousie University, B3H 4R2 Halifax, Canada

Complete contact information is available at: https://pubs.acs.org/10.1021/acs.jpclett.1c00158

Notes

The authors declare no competing financial interest.

ACKNOWLEDGMENTS

E.G. is grateful for support from NSF via Grant CHE-1800325. This research was supported in part through computational resources and services provided by Advanced Research Computing – Technology Services (ARC-TS), a division of

Information and Technology Services (ITS) at the University of Michigan, Ann Arbor.

REFERENCES

- (1) Lidzey, D.; Bradley, D.; Armitage, A.; Walker, S.; Skolnick, M. Photon-mediated hybridization of frenkel excitons in organic semiconductor microcavities. *Science* **2000**, 288, 1620–1623.
- (2) Tischler, J.; Bradley, M.; Bulović, V.; Song, J.; Nurmikko, A. Strong Coupling in a Microcavity LED. *Phys. Rev. Lett.* **2005**, 95, 036401.
- (3) Kéna-Cohen, S.; Davanço, M.; Forrest, S. Strong Exciton-Photon Coupling in an Organic Single Crystal Microcavity. *Phys. Rev. Lett.* **2008**, *101*, 116401.
- (4) Kéna-Cohen, S.; Forrest, S. Room-temperature polariton lasing in an organic single-crystal microcavity. *Nat. Photonics* **2010**, *4*, 371–375
- (5) Hutchison, J.; Liscio, A.; Schwartz, T.; Canaguier-Durand, A.; Genet, C.; Palermo, V.; Samorì, P.; Ebbesen, T. Tuning the Work-Function Via Strong Coupling. *Adv. Mater.* **2013**, *25*, 2481–2485.
- (6) Bellessa, J.; Symonds, C.; Laverdant, J.; Benoit, J.-M.; Plenet, J.; Vignoli, S. Strong Coupling between Plasmons and Organic Semiconductors. *Electronics* **2014**, *3*, 303–313.
- (7) Schwartz, T.; Hutchison, J.; Genet, C.; Ebbesen, T. Reversible Switching of Ultrastrong Light-Molecule Coupling. *Phys. Rev. Lett.* **2011**, *106*, 196405–4.
- (8) Kéna-Cohen, S.; Maier, S.; Bradley, D. Ultrastrongly Coupled Exciton-Polaritons in Metal-Clad Organic Semiconductor Microcavities. *Adv. Opt. Mater.* **2013**, *1*, 827–833.
- (9) Mazzeo, M.; Genco, A.; Gambino, S.; Ballarini, D.; Mangione, F.; Di Stefano, O.; Patanè, S.; Savasta, S.; Sanvitto, D.; Gigli, G. Ultrastrong light-matter coupling in electrically doped microcavity organic light emitting diodes. *Appl. Phys. Lett.* **2014**, *104*, 233303–5.
- (10) George, J.; Wang, S.; Chervy, T.; Canaguier-Durand, A.; Schaeffer, G.; Lehn, J.-M.; Hutchison, J.; Genet, C.; Ebbesen, T. Ultra-strong coupling of molecular materials: Spectroscopy and dynamics. *Faraday Discuss.* **2015**, *178*, 281–294.
- (11) Dirac, P. A. M. The principles of quantum mechanics; Clarendon Press: Oxford, 1958.
- (12) Louisell, W. H. Radiation and Noise in Quantum Electronics; McGraw-Hill: New York, 1964.
- (13) Loudon, R. The quantum theory of light; Oxford University Press: New York, 1986.
- (14) Walther, H.; Varcoe, B.; Englert, B.-G.; Becker, T. Cavity quantum electrodynamics. *Rep. Prog. Phys.* **2006**, *69*, 1325–1382.
- (15) Andrew, P.; Barnes, W. L. Förster energy transfer in an optical microcavity. *Science* **2000**, *290*, 785–788.
- (16) Hutchison, J.; Schwartz, T.; Genet, C.; Devaux, E.; Ebbesen, T. Modifying Chemical Landscapes by Coupling to Vacuum Fields. *Angew. Chem., Int. Ed.* **2012**, *51*, 1592–1596.
- (17) Törmä, P.; Barnes, W. Strong coupling between surface plasmon polaritons and emitters: A review. *Rep. Prog. Phys.* **2015**, 78, 013901–35.
- (18) Flick, J.; Ruggenthaler, M.; Appel, H.; Rubio, A. Kohn—Sham approach to quantum electrodynamical density-functional theory: Exact time-dependent effective potentials in real space. *Proc. Natl. Acad. Sci. U. S. A.* **2015**, *112*, 15285—15290.
- (19) Feist, J.; Garcia-Vidal, F. Extraordinary Exciton Conductance Induced by Strong Coupling. *Phys. Rev. Lett.* **2015**, *114*, 196402–5.
- (20) Schachenmayer, J.; Genes, C.; Tignone, E.; Pupillo, G. Cavity-Enhanced Transport of Excitons. *Phys. Rev. Lett.* **2015**, *114*, 196403–6.
- (21) Shalabney, A.; George, J.; Hutchison, J.; Pupillo, G.; Genet, C.; Ebbesen, T. Coherent coupling of molecular resonators with a microcavity mode. *Nat. Commun.* **2015**, *6*, 5981.
- (22) Orgiu, E.; George, J.; Hutchison, J.; Devaux, E.; Dayen, J.; Doudin, B.; Stellacci, F.; Genet, C.; Schachenmayer, J.; Genes, C.; et al. Conductivity in organic semiconductors hybridized with the vacuum field. *Nat. Mater.* **2015**, *14*, 1123–1129.

- (23) Long, J.; Simpkins, B. Coherent Coupling between a Molecular Vibration and Fabry–Perot Optical Cavity to Give Hybridized States in the Strong Coupling Limit. *ACS Photonics* **2015**, *2*, 130–136.
- (24) Ebbesen, T. Hybrid Light-Matter States in a Molecular and Material Science Perspective. Acc. Chem. Res. 2016, 49, 2403-2412.
- (25) Thomas, A.; George, J.; Shalabney, A.; Dryzhakov, M.; Varma, S.; Moran, J.; Chervy, T.; Zhong, X.; Devaux, E.; Genet, C.; et al. Ground-State Chemical Reactivity under Vibrational Coupling to the Vacuum Electromagnetic Field. *Angew. Chem.* **2016**, *128*, 11634–11638.
- (26) Zhong, X.; Chervy, T.; Wang, S.; George, J.; Thomas, A.; Hutchison, J.; Devaux, E.; Genet, C.; Ebbesen, T. Non-Radiative Energy Transfer Mediated by Hybrid Light-Matter States. *Angew. Chem.* **2016**, *128*, 6310–6314.
- (27) Herrera, F.; Spano, F. Cavity-Controlled Chemistry in Molecular Ensembles. *Phys. Rev. Lett.* **2016**, *116*, 238301–6.
- (28) Casey, S.; Sparks, J. Vibrational Strong Coupling of Organometallic Complexes. J. Phys. Chem. C 2016, 120, 28138—28143
- (29) Sanvitto, D.; Kéna-Cohen, S. The road towards polaritonic devices. *Nat. Mater.* **2016**, *15*, 1061–1073.
- (30) Kowalewski, M.; Bennett, K.; Mukamel, S. Cavity Femtochemistry: Manipulating Nonadiabatic Dynamics at Avoided Crossings. *J. Phys. Chem. Lett.* **2016**, *7*, 2050–2054.
- (31) Kowalewski, M.; Bennett, K.; Mukamel, S. Non-adiabatic dynamics of molecules in optical cavities. *J. Chem. Phys.* **2016**, *144*, 054309–9.
- (32) Flick, J.; Ruggenthaler, M.; Appel, H.; Rubio, A. Atoms and molecules in cavities, from weak to strong coupling in quantum-electrodynamics (QED) chemistry. *Proc. Natl. Acad. Sci. U. S. A.* **2017**, *114*, 3026–3034.
- (33) Zhong, X.; Chervy, T.; Zhang, L.; Thomas, A.; George, J.; Genet, C.; Hutchison, J.; Ebbesen, T. Energy Transfer between Spatially Separated Entangled Molecules. *Angew. Chem., Int. Ed.* **2017**, *56*, 9034–9038.
- (34) Martínez-Martínez, L.; Ribeiro, R.; Campos-González-Angulo, J.; Yuen-Zhou, J. Can Ultrastrong Coupling Change Ground-State Chemical Reactions? *ACS Photonics* **2018**, *5*, 167–176.
- (35) Fregoni, J.; Granucci, G.; Coccia, E.; Persico, M.; Corni, S. Manipulating azobenzene photoisomerization through strong lightmolecule coupling. *Nat. Commun.* **2018**, *9*, 4688.
- (36) Sáez-Blázquez, R.; Feist, J.; Fernández-Domínguez, A.; García-Vidal, F. Organic polaritons enable local vibrations to drive long-range energy transfer. *Phys. Rev. B: Condens. Matter Mater. Phys.* **2018**, 97, 241407–5.
- (37) Flick, J.; Welakuh, D.; Ruggenthaler, M.; Appel, H.; Rubio, A. Light–Matter Response in Nonrelativistic Quantum Electrodynamics. *ACS Photonics* **2019**, *6*, 2757–2778.
- (38) Galego, J.; Climent, C.; Garcia-Vidal, F.; Feist, J. Cavity Casimir-Polder Forces and Their Effects in Ground-State Chemical Reactivity. *Phys. Rev. X* **2019**, *9*, 021057.
- (39) Lather, J.; Bhatt, P.; Thomas, A.; Ebbesen, T.; George, J. Cavity Catalysis by Cooperative Vibrational Strong Coupling of Reactant and Solvent Molecules. *Angew. Chem., Int. Ed.* **2019**, *58*, 10635–10638.
- (40) Schäfer, C.; Ruggenthaler, M.; Appel, H.; Rubio, A. Modification of excitation and charge transfer in cavity quantum-electrodynamical chemistry. *Proc. Natl. Acad. Sci. U. S. A.* **2019**, *116*, 4883–4892.
- (41) Hoffmann, N.; Schäfer, C.; Rubio, A.; Kelly, A.; Appel, H. Capturing vacuum fluctuations and photon correlations in cavity quantum electrodynamics with multitrajectory Ehrenfest dynamics. *Phys. Rev. A: At., Mol., Opt. Phys.* **2019**, *99*, 063819–9.
- (42) Hoffmann, N.; Schäfer, C.; Säkkinen, N.; Rubio, A.; Appel, H.; Kelly, A. Benchmarking semiclassical and perturbative methods for real-time simulations of cavity-bound emission and interference. *J. Chem. Phys.* **2019**, *151*, 244113–14.
- (43) Lacombe, L.; Hoffmann, N.; Maitra, N. Exact Potential Energy Surface for Molecules in Cavities. *Phys. Rev. Lett.* **2019**, *123*, 083201–

- (44) Mandal, A.; Huo, P. Investigating New Reactivities Enabled by Polariton Photochemistry. *J. Phys. Chem. Lett.* **2019**, *10*, 5519–5529.
- (45) Hoffmann, N.; Lacombe, L.; Rubio, A.; Maitra, N. Effect of Many Modes on Self-Polarization and Photochemical Suppression in Cavities. *arXiv* (Mesoscale and Nanoscale Physics), July 14, 2020. https://arxiv.org/abs/2001.07330
- (46) Flick, J.; Rivera, N.; Narang, P. Strong light-matter coupling in quantum chemistry and quantum photonics. *Nanophotonics* **2018**, *7*, 1479–1501.
- (47) Gu, B.; Mukamel, S. Manipulating nonadiabatic conical intersection dynamics by optical cavities. *Chem. Sci.* **2020**, *11*, 1290–1298.
- (48) Mandal, A.; Krauss, T.; Huo, P. Polariton-Mediated Electron Transfer via Cavity Quantum Electrodynamics. *J. Phys. Chem. B* **2020**, *124*, 6321–6340.
- (49) Dicke, R. Coherence in spontaneous radiation processes. *Phys. Rev.* **1954**, 93, 99–110.
- (50) Jaynes, E.; Cummings, F. Comparison of quantum and semiclassical radiation theories with application to the beam maser. *Proc. IEEE* **1963**, *51*, 89–109.
- (51) Tavis, M.; Cummings, F. Approximate solutions for an N-molecule-radiation-field Hamiltonian. *Phys. Rev.* **1969**, *188*, 692–695.
- (52) Houdre, R.; Stanley, R.; Ilegems, M. Vacuum-field Rabi splitting in the presence of inhomogeneous broadening: Resolution of a homogeneous linewidth in an inhomogeneously broadened system. *Phys. Rev. A: At., Mol., Opt. Phys.* **1996**, *53*, 2711–2715.
- (53) Garraway, B. The Dicke model in quantum optics: Dicke model revisited. P. R. Soc. A: Math. Phys. 2011, 369, 1137–1155.
- (54) Stock, G.; Thoss, M. Classical description of nonadiabatic quantum dynamics. *Adv. Chem. Phys.* **2005**, *131*, 243–376.
- (55) Meyer, H.; Miller, W. A classical analog for electronic degrees of freedom in nonadiabatic collision processes. *J. Chem. Phys.* **1979**, 70, 3214–3223.
- (56) Stock, G.; Thoss, M. Semiclassical Description of Nonadiabatic Quantum Dynamics. *Phys. Rev. Lett.* **1997**, *78*, 578–581.
- (57) Sun, X.; Wang, H.; Miller, W. Semiclassical theory of electronically nonadiabatic dynamics: Results of a linearized approximation to the initial value representation. *J. Chem. Phys.* **1998**, *109*, 7064.
- (58) Wang, H.; Song, X.; Chandler, D.; Miller, W. Semiclassical study of electronically nonadiabatic dynamics in the condensed phase: Spin-boson problem with Debye spectral density. *J. Chem. Phys.* **1999**, *110*, 4828–4840.
- (59) Swenson, D.; Levy, T.; Cohen, G.; Rabani, E.; Miller, W. Application of a semiclassical model for the second-quantized many-electron Hamiltonian to nonequilibrium quantum transport: The resonant level model. *J. Chem. Phys.* **2011**, *134*, 164103–9.
- (60) Cotton, S.; Miller, W. Symmetrical windowing for quantum states in quasi-classical trajectory simulations: Application to electronically non-adiabatic processes. *J. Chem. Phys.* **2013**, *139*, 234112–10.
- (61) Cotton, S.; Miller, W. Symmetrical Windowing for Quantum States in Quasi-Classical Trajectory Simulations. *J. Phys. Chem. A* **2013**, *117*, 7190–7194.
- (62) Cotton, S.; Igumenshchev, K.; Miller, W. Symmetrical windowing for quantum states in quasi-classical trajectory simulations: Application to electron transfer. *J. Chem. Phys.* **2014**, *141*, 084104–11.
- (63) Cotton, S.; Miller, W. A Symmetrical Quasi-Classical Spin-Mapping Model for the Electronic Degrees of Freedom in Non-Adiabatic Processes. *J. Phys. Chem. A* **2015**, *119*, 12138–12145.
- (64) Cotton, S.; Miller, W. The Symmetrical Quasi-Classical Model for Electronically Non-Adiabatic Processes Applied to Energy Transfer Dynamics in Site-Exciton Models of Light-Harvesting Complexes. J. Chem. Theory Comput. 2016, 12, 983–991.
- (65) Cotton, S.; Miller, W. A new symmetrical quasi-classical model for electronically non-adiabatic processes: Application to the case of weak non-adiabatic coupling. *J. Chem. Phys.* **2016**, *145*, 144108–17.

- (66) Saller, M.; Kelly, A.; Richardson, J. On the identity of the identity operator in nonadiabatic linearized semiclassical dynamics. *J. Chem. Phys.* **2019**, *150*, 071101–8.
- (67) Saller, M.; Kelly, A.; Richardson, J. Improved population operators for multi-state nonadiabatic dynamics with the mixed quantum-classical mapping approach. *Faraday Discuss.* **2020**, 221, 150–167.
- (68) Gao, X.; Saller, M.; Liu, Y.; Kelly, A.; Richardson, J.; Geva, E. Benchmarking Quasiclassical Mapping Hamiltonian Methods for Simulating Electronically Nonadiabatic Molecular Dynamics. *J. Chem. Theory Comput.* **2020**, *16*, 2883–2895.
- (69) Tao, G. Electronically Nonadiabatic Dynamics in Singlet Fission: A Quasi-Classical Trajectory Simulation. *J. Phys. Chem. C* **2014**, *118*, 17299–17305.
- (70) Tao, G. A multi-state trajectory method for non-adiabatic dynamics simulations. *J. Chem. Phys.* **2016**, *144*, 094108–9.
- (71) Tao, G.; Shen, N. Mapping State Space to Quasiclassical Trajectory Dynamics in Coherence-Controlled Nonadiabatic Simulations for Condensed Phase Problems. *J. Phys. Chem. A* **2017**, *121*, 1734–1747.
- (72) Tao, G. Nonadiabatic Dynamics of Hydrogen Diffusion on Cu(001): Classical Mapping Model with Multistate Projection Window in Real Space. *ChemPhysChem* **2019**, *20*, 2127–2135.
- (73) Liu, J. A unified theoretical framework for mapping models for the multi-state Hamiltonian. *J. Chem. Phys.* **2016**, *145*, 204105–15.
- (74) He, X.; Liu, J. A new perspective for nonadiabatic dynamics with phase space mapping models. *J. Chem. Phys.* **2019**, *151*, 024105–22.
- (75) Runeson, J.; Richardson, J. Spin-mapping approach for nonadiabatic molecular dynamics. *J. Chem. Phys.* **2019**, *151*, 044119–14.
- (76) Runeson, J. E.; Richardson, J. O. Generalized spin mapping for quantum-classical dynamics. *J. Chem. Phys.* **2020**, *152*, 084110.
- (77) Wang, H.; Thoss, M.; Miller, W. H. Forward-backward initial value representation for the calculation of thermal rate constants for reactions in complex molecular systems. *J. Chem. Phys.* **2000**, *112*, 47–55.
- (78) Shi, Q.; Geva, E. A relationship between semiclassical and centroid correlation functions. *J. Chem. Phys.* **2003**, *118*, 8173–8184. (79) Shi, Q.; Geva, E. Nonradiative electronic relaxation rate
- constants from approximations based on linearizing the path-integral forward-backward action. *J. Phys. Chem. A* **2004**, *108*, 6109–6116.
- (80) Shi, Q.; Geva, E. A semiclassical generalized quantum master equation for an arbitrary system-bath coupling. *J. Chem. Phys.* **2004**, *120*, 10647–10658.
- (81) McLachlan, A. A variational solution of the time-dependent Schrodinger equation. *Mol. Phys.* **1964**, *8*, 39–44.
- (82) Liu, Y.; Gao, X.; Lai, Y.; Mulvihill, E.; Geva, E. Electronic Dynamics through Conical Intersections via Quasiclassical Mapping Hamiltonian Methods. *J. Chem. Theory Comput.* **2020**, *16*, 4479–4488
- (83) Flick, J.; Appel, H.; Ruggenthaler, M.; Rubio, A. Cavity Born-Oppenheimer Approximation for Correlated Electron-Nuclear-Photon Systems. *J. Chem. Theory Comput.* **2017**, *13*, 1616–1625.
- (84) Cotton, S.; Liang, R.; Miller, W. On the adiabatic representation of Meyer-Miller electronic-nuclear dynamics. *J. Chem. Phys.* **2017**, 147, 064112–11.
- (85) Hillery, M.; O'Connell, R. F.; Scully, M. O.; Wigner, E. P. Distribution functions in physics: Fundamentals. *Phys. Rep.* **1984**, *106*, 121–167.
- (86) Kelly, A.; van Zon, R.; Schofield, J.; Kapral, R. Mapping quantum-classical Liouville equation: Projectors and trajectories. *J. Chem. Phys.* **2012**, *136*, 084101–13.
- (87) Kim, H.; Nassimi, A.; Kapral, R. Quantum-classical Liouville dynamics in the mapping basis. *J. Chem. Phys.* **2008**, 129, 084102–6. (88) Su, Q.; Eberly, J. H. Model atom for multiphoton physics. *Phys. Rev. A: At., Mol., Opt. Phys.* **1991**, 44, 5997–6008.

- (89) Buzek, V.; Drobny, G.; Kim, M.; Havukainen, M.; Knight, P. Numerical simulations of atomic decay in cavities and material media. *Phys. Rev. A: At., Mol., Opt. Phys.* **1999**, *60*, 582–592.
- (90) Tully, J. Molecular dynamics with electronic transitions. J. Chem. Phys. 1990, 93, 1061–1071.
- (91) Gao, X.; Lai, Y.; Geva, E. Simulating Absorption Spectra of Multiexcitonic Systems via Quasiclassical Mapping Hamiltonian Methods. *J. Chem. Theory Comput.* **2020**, *16*, 6465–6480.
- (92) Kosloff, R. Propagation methods for quantum molecular dynamics. *Annu. Rev. Phys. Chem.* **1994**, *45*, 145–178.
- (93) Meyer, H.-D.; Gatti, F.; Worth, G. Multidimensional Quantum Dynamics; MCTDH Theory and Applications; John Wiley & Sons, 2009.
- (94) Greene, S.; Batista, V. Tensor-Train Split-Operator Fourier Transform (TT-SOFT) Method: Multidimensional Nonadiabatic Quantum Dynamics. *J. Chem. Theory Comput.* **2017**, *13*, 4034–4042.